

# BIOSIGNATURE ANISOTROPY MODELED ON TEMPERATE TIDALLY LOCKED M-DWARF PLANETS

HOWARD CHEN,<sup>1,2</sup> ERIC T. WOLF,<sup>3,4</sup> RAVI KOPPARAPU,<sup>4,5</sup> SHAWN DOMAGAL-GOLDMAN,<sup>4,5</sup> AND DANIEL E. HORTON<sup>1,2</sup>

<sup>1</sup>*Department of Earth and Planetary Sciences, Northwestern University, Evanston, IL 60202, USA*

<sup>2</sup>*Center for Interdisciplinary Exploration & Research in Astrophysics (CIERA), Evanston, IL 60202, USA*

<sup>3</sup>*Laboratory for Atmospheric and Space Physics, Department of Atmospheric and Oceanic Sciences, University of Colorado Boulder, Boulder, CO 80309, USA*

<sup>4</sup>*NASA Astrobiology Institute Virtual Planetary Laboratory, Seattle, WA 98194, USA*

<sup>5</sup>*NASA Goddard Spaceflight Center, Greenbelt, MD 20771, USA*

## ABSTRACT

A planet’s atmospheric constituents (e.g., O<sub>2</sub>, O<sub>3</sub>, H<sub>2</sub>O<sub>v</sub>, CO<sub>2</sub>, CH<sub>4</sub>, and N<sub>2</sub>O) can provide clues to its surface habitability, and may offer biosignature targets for remote life detection efforts. The plethora of rocky exoplanets found by recent transit surveys (e.g., the *Kepler* mission) indicates that potentially habitable systems orbiting K- and M-dwarf stars may have very different orbital and atmospheric characteristics than Earth. To assess the physical distribution and observational prospects of various biosignatures and habitability indicators, it is important to understand how they may change under different astrophysical and geophysical configurations, and to simulate these changes with models that include feedbacks between different subsystems of a planet’s climate. Here we use a three-dimensional (3D) Chemistry-Climate model (CCM) to study the effects of changes in stellar spectral energy distribution (SED), stellar activity, and planetary rotation on Earth-analogs and tidally-locked planets. Our simulations show that, apart from shifts in stellar SEDs and UV radiation, changes in illumination geometry and rotation-induced circulation can influence the global distribution of atmospheric biosignatures. We find that the stratospheric day-to-nightside mixing ratio differences on tidally-locked planets remain low (< 20%) across the majority of the canonical biosignatures. Interestingly however, secondary photosynthetic biosignatures (e.g., C<sub>2</sub>H<sub>6</sub>S) show much greater (~67%) day-to-nightside differences, and point to regimes in which tidal-locking could have observationally distinguishable effects on phase curve, transit, and secondary eclipse measurements. Overall, this work highlights the potential and promise for 3D CCMs to study the atmospheric properties and habitability of terrestrial worlds.

*Keywords:* astrobiology – planets and satellites: atmospheres – planets and satellites: terrestrial planets

## 1. INTRODUCTION

A promising approach in the hunt for life beyond Earth is through the detection of biosignatures – biologically produced compounds such as  $O_2$ ,  $O_3$ ,  $CH_4$ ,  $N_2O$ , and  $CO_2$  – in the atmospheres of terrestrial planets orbiting the putative habitable zones (HZs) of nearby stars (Lovelock 1975; Sagan et al. 1993; Seager et al. 2009; Kasting et al. 2015).

In recent years, the convergence of our ability to detect, confirm, and characterize extrasolar planets has profoundly strengthened the prospects of finding life on other worlds. Consistently improving measurements of stellar mass, radius, and distance allows more accurate constraints on their attending planets (Mann et al. 2015). Large-scale observational surveys such as the M-Earth project, TRAPPIST survey, Hungarian Automated Telescope Network (HATNet), Kepler Space Telescope, and Transiting Exoplanet Satellite Survey (TESS) have detected planets in the habitable zones around these stars (Thompson et al. 2018) and will continue to monitor closer and brighter systems for Earth-sized planets (Barclay et al. 2018). Simultaneously, follow-up characterization efforts of these confirmed planets were able to resolve atmospheres of much smaller planets than past efforts (e.g., HAT-P-26b; Wakeford et al. 2017). Looking ahead, a variety of instruments are being designed with life detection goals in mind. This includes ground-based observatories such as the European Extremely Large Telescope (E-ELT), Giant Magellan Telescope (GMT), and Thirty-Meter Telescope (TMT), as well as space-based missions such as the James Webb Space Telescope (JWST), Large UV/Optical/IR Surveyor (LUVOIR), Origins Space Telescope (OST), and Habitable Exoplanet Imaging Observatory (HabEx). HabEx and LUVOIR in particular would enable characterization of potentially habitable Earth-sized rocky planets in our solar neighborhood ( $\lesssim 100$  parsecs; Bolcar et al. 2016; Mennesson et al. 2016; Batalha et al. 2018).

The recent discoveries of Proxima Centauri b (Anglada-Escudé et al. 2016) and the TRAPPIST-1 system (Gillon et al. 2017) demonstrate that analyses of small rocky planets are within reach. However, many of these planets orbit extremely close to their host M-type stars (0.02-0.2 AU) and are susceptible to trapping by tidal forces (Tarter et al. 2007). Tidally-locked but potentially habitable planets are expected to be common in HZs of low-mass stars ( $\sim 15\%$ ; Dressing and Charbonneau 2015) – which dominate our solar neighborhood stellar population ( $\sim 70\%$ ; Henry et al. 2006). Concurrently, our earliest opportunity for a biosignature search will likely come from the JWST and ground-

based extremely large telescopes (E-ELT, GMT, and TMT); these observatories will enable spectroscopic observations of rocky planets around K- and M-type stars. It is therefore likely that our first opportunity to measure atmospheres of rocky worlds will be tidally-locked terrestrial planets around K- or M-dwarf stars.

Characterization of exoplanets primarily involves measuring starlight and terrestrial thermal emissions absorbed by planetary atmospheres as a function of wavelength. For transit spectroscopy, which will be the main tool for obtaining spectra from planets around M-dwarf stars, observations are biased towards atmospheric constituents across the terminators. Therefore, interpreting spectroscopic observations requires inferring both the concentration and distribution of detectable gases. Such properties can be predicted by 3D global climate and chemistry-climate models (GCMs and CCMs). GCMs and CCMs are numerical models that employ laws of physics, fluid motion, and in the case of CCMs, chemistry to simulate movements, interactions, and climatic implications of a planet’s atmospheric constituents and boundary conditions.

Previous simulations of atmospheres of tidally-locked planets performed with 3D GCMs have demonstrated that habitable states of tidally-locked planets are strong functions of: (i) Coriolis force (Yang et al. 2016; Way et al. 2016; Kopparapu et al. 2016), (ii) stellar energy distribution (SED) and bolometric stellar flux (Kopparapu et al. 2017; Wolf 2017), (iii) atmospheric mass (Wordsworth 2015), and (iv) radiative transfer scheme (Yang et al. 2016). Despite the ability of GCMs to simulate key climatological factors, as demonstrated by these studies, their foci have primarily been on questions of habitability, rather than the concentrations and distributions of biologically-produced gases and habitability indicators.

To study effects of tidal-locking on atmospheric chemistry and molecular spectroscopic signals, models capable of resolving chemical speciation, reactions, and transport are needed. To date, exoplanet atmospheric photochemical predictions have largely relied on one-dimensional global-mean photochemistry-climate models (e.g., Kasting et al. 1984; Segura et al. 2005; Meadows et al. 2018). These 1D models have been used to simulate synthetic spectra of hypothetical rocky planets under the influence of different host SEDs (Rauer et al. 2011; Rugheimer et al. 2015). However, 1D models employ relatively simple eddy-diffusion parameterizations for vertical transport and do not account for atmospheric dynamics, climate heterogeneities, or 3D geometric effects critical to observations. These factors are important as advection and diffusion can affect con-

centration, distribution, and ultimately the composition of an atmosphere (Seinfeld and Pandis 2012). In addition to altering photochemistry, as shown by 1D models, shifts in stellar SED can influence atmospheric circulation and climate (e.g., Shields et al. 2014; Fujii et al. 2017). Atmospheric chemistry and dynamics are thus interactive, and should ideally be simulated using fully-coupled 3D model components.

Here, to better understand the observational potential of tidally-locked planets, the integrated effects of atmospheric chemistry, photochemistry, and circulation are considered over the 3D geometry of a planet’s atmosphere. In this Letter, we simulate Earth-analogs and tidally-locked planets around M-dwarf stars using a 3D CCM, while seeking to (i) elucidate the photochemical nature of Earth-like worlds, (ii) demonstrate the utility of 3D CCMs in terrestrial exoplanet studies, (iii) and advance model comparison efforts between 3D and 1D research communities.

## 2. MODEL DESCRIPTION & EXPERIMENTAL SETUP

In this study, we employ the Community Atmosphere Model with Chemistry (CAM-chem), a subset of the National Center for Atmospheric Research (NCAR) Community Earth System Model (CESM v.1.2), to investigate atmospheres of Earth-like planets. CAM-chem is a 3D global CCM that simulates interactions of atmospheric chemistry, radiation, thermodynamics, and dynamics (for complete model description see Lamarque et al. (2012)). CAM-chem combines the CAM4 atmospheric component with the fully implemented Model for Ozone and Related Chemical Tracers (MOZART) chemical transport model. CAM-chem resolves 97 gas phase species and aerosols linked by 196 chemical and photolytic reactions. CAM, the atmosphere component of the model, has seen wide applications in problems of paleoclimate and exoplanets (e.g., Wolf and Toon 2015; Kopparapu et al. 2016), whereas CAM-chem has largely been limited to studies of present Earth. All simulations presented were run for 30 Earth years and reported results are averaged over the last 20.

We simulate Earth-analogs and tidally-locked planets and assess the sensitivity of atmospheric biosignatures to three primary variables: (i) stellar spectral energy distribution, (ii) stellar UV radiation, and (iii) planetary rotation period. To simulate Earth-analogs, we use a preindustrial Earth setup forced by solar spectral irradiance data (Lean et al. 1995), i.e., apart from the orbital parameters described below, our Earth-analog simulation uses identical boundary and initial conditions to Earth in 1850, prior to anthropogenic influences (Taylor

et al. 2012). These conditions include atmospheric gases  $N_2$  (78% by volume),  $O_2$  (21%), and  $CO_2$  ( $2.85 \times 10^{-2}\%$ ) (MacFarling Meure et al. 2006). In addition, the model simulates the free-running evolution of  $H_2O_v$  and  $O_3$ , while  $CH_4$  and  $N_2O$  surface fluxes are latitudinally variable (global mean  $CH_4$ :  $7.23 \times 10^{-7}$  and  $N_2O$ :  $2.73 \times 10^{-7}$  mol mol $^{-1}$ ). Throughout the remainder of the paper, we refer to this Earth-Sun simulation as the baseline.

We also modify CAM-chem to simulate tidally-locked planets with initially Earth-like atmospheric compositions forced by M-dwarf SEDs. This SED was obtained from an open-source dataset of an M6V star, Proxima Centauri, compiled by NASA’s Virtual Planetary Laboratory (VPL) team and is available at <http://vpl.astro.washington.edu/spectra/stellar/>. We explore two SED-types (active and quiescent) that bracket the endmember ranges of stellar activity. VPL Proxima Cen. data is assumed to be moderately-to-highly active. To construct a quiescent M-dwarf SED, we swap out UV bands ( $\lambda < 500$  nm) of the original Proxima Cen. data with that of a low-activity star (HD114710). For all exo-Earth simulations, we assume tidal-locking (i.e., trapped in 1:1 spin-orbit resonances), with orbital periods of 50 Earth days. While we do not use self-consistent stellar-flux orbital period relationships (e.g., Kopparapu et al. 2016; Haqq-Misra et al. 2018), the idealized case studied here highlights the value of using CCMs for modeling chemical processes on slowly and synchronously rotating planets.

For both Earth and tidally-locked exoplanet simulations, we set orbital parameters (obliquity, eccentricity, and precession) to zero, such that top-of-atmosphere incident stellar flux is symmetric about the equator. Incident bolometric stellar flux for all simulations is set to 1360 W m $^{-2}$ . The substellar point for all simulations is fixed at (Earths) latitude = 0° and longitude = 180°, in the Pacific Ocean. Note that other studies (e.g., Lewis et al. 2018) have shown that surface type beneath a substellar point can modify water vapor availability, influencing water vapor-induced greenhouse and cloud radiative effects, and possibly atmospheric chemistry.

In all simulations, we assume present Earths continental configuration, topography, mass, and radius. We use prognostic atmospheric and oceanic components of CESM, as well as prescribed preindustrial land, surface ice, and sea ice components. Horizontal resolution (latitude  $\times$  longitude) is set to  $1.9^\circ \times 2.5^\circ$  with 26 vertical atmospheric levels and model top of 1 mb ( $\sim 50$  km). The land model is Community Land Model version 4.0 with non-interactive surface features. The ocean component is a thermodynamic slab model with prescribed

**Table 1. Model Comparisons of Approximate Global-mean Mixing Ratios of Various Gases**

Study	Rauer et al. (2011)	Rugheimer et al. (2015)	This work
Model	1D photochemical	EXO-P	NCAR's CAM-chem
SED data	AD Leonis <sup>a</sup>	active M6 stellar model <sup>b</sup>	Proxima Cen. <sup>c</sup>
Bond Albedo	N/A <sup>d</sup>	0.07	0.46
$T_{\text{surf}}$ (K)	298	300	242
$\text{O}_{3,\text{surf}}$ (mol mol <sup>-1</sup> )	$8 \times 10^{-11}$	$10^{-9}$	$9.4 \times 10^{-13}$
$\text{CH}_{4,\text{surf}}$ (mol mol <sup>-1</sup> )	$10^{-4}$	$1 \times 10^{-3}$	$3.4 \times 10^{-4}$
$\text{N}_2\text{O}_{\text{surf}}$ (mol mol <sup>-1</sup> )	$2.0 \times 10^{-6}$	$1.7 \times 10^{-6}$	$2.4 \times 10^{-6}$
$\text{H}_2\text{O}_{\text{surf}}$ (mol mol <sup>-1</sup> )	$7.0 \times 10^{-2}$	$5.0^{-2}$	$3.5 \times 10^{-4}$
$T_{100\text{mb}}^e$ (K)	251	245	200
$\text{O}_{3,100\text{mb}}$ (mol mol <sup>-1</sup> )	$10^{-8}$	$10^{-6}$	$5.2 \times 10^{-7}$
$\text{CH}_{4,100\text{mb}}$ (mol mol <sup>-1</sup> )	$10^{-6}$	$1 \times 10^{-3}$	$3.1 \times 10^{-4}$
$\text{N}_2\text{O}_{100\text{mb}}$ (mol mol <sup>-1</sup> )	$10^{-5}$	$5 \times 10^{-7}$	$2.0 \times 10^{-6}$
$\text{H}_2\text{O}_{100\text{mb}}$ (mol mol <sup>-1</sup> )	$10^{-7}$	$7.0 \times 10^{-4}$	$5.8 \times 10^{-6}$

Approximate atmospheric temperature (units of K) and mixing ratios of various gas phase species (units of mol mol<sup>-1</sup>) simulated on Earth-like planets by various authors. All data reported are taken from simulations forced by active stellar SEDs that range from M6V to M8V dwarf stars. <sup>a</sup>Active M3.5eV star,  $T_{\text{eff}} = 3300$  K,  $M = 0.41M_{\odot}$ . <sup>b</sup>Part of a suite of stellar SED model data generated by [Rugheimer et al. \(2015\)](#) to represent the most active M-dwarf observations (e.g., PHOENIX or MUSCLES database). <sup>c</sup>SED data from Virtual Planetary Laboratory's stellar spectrum database ([Meadows et al. 2018](#)). <sup>d</sup>Data not provided. <sup>e</sup>Values reported at 100 mb.

heat flux values sourced from dynamical ocean simulations (e.g., [Danabasoglu and Gent 2009](#)).

Consistent with 1D studies (e.g., [Segura et al. 2005](#)) and in alignment with our lack of terrestrial exoplanet observations, we assume atmospheric compositions, biological production, and dry deposition rates of gaseous species the same as those of preindustrial Earth. Apart from  $\text{CH}_4$  and  $\text{N}_2\text{O}$ , global surface gas flux inputs are based on spatially-explicit preindustrial monthly averages (e.g., DMS; [Kettle and Andreae 2000](#)). Due to SED sensitivities,  $\text{CH}_4$  and  $\text{N}_2\text{O}$  surface flux boundary conditions are estimated via ancillary CCM simulations that allow for the emergence of stellar SED-dependent flux magnitudes (i.e., WACCM; [Neale et al. 2010](#)). Emergent SED-consistent  $\text{N}_2\text{O}$  and  $\text{CH}_4$  flux estimates are temporally and spatially fixed in active and quiescent M-dwarf simulations at  $\text{CH}_4$ :  $3.5 \times 10^{-4}$  and  $2.3 \times 10^{-3}$  mol mol<sup>-1</sup> and  $\text{N}_2\text{O}$ :  $2.5 \times 10^{-6}$  and  $3.2 \times 10^{-5}$  mol mol<sup>-1</sup>, respectively. Given uncertainties inherent in flux estimates, sensitivity experiment and day-to-night side mixing ratio comparisons should focus on relative rather than absolute differences.

### 3. RESULTS

Three general observations can be made from our simulated 3D global distributions of  $\text{O}_3$ ,  $\text{CH}_4$ ,  $\text{N}_2\text{O}$ , and DMS on Earth-like and tidally-locked planets (Figures 1 and 4): (i) Changes in mixing ratios of  $\text{O}_3$ ,  $\text{CH}_4$ , and  $\text{N}_2\text{O}$  are primarily due to different levels of stellar UV flux amongst the three SED datasets. (ii) Introduction of tidal-locking modifies globally homogeneous gas distributions that characterize Earth-like scenarios. (iii) Heterogeneous surface-to-atmosphere flux distributions (e.g., DMS) can influence the resultant mixing ratios of atmospheric constituents.

To facilitate analysis of our results, we define a day-to-night side mixing (mole) ratio contrast as:

$$r_{\text{diff}} = \frac{r_{\text{day}} - r_{\text{night}}}{r_{\text{globe}}} \quad (1)$$

i.e., the relative difference between the two hemispheres, where  $r_{\text{day}}$  is the dayside hemispheric mixing



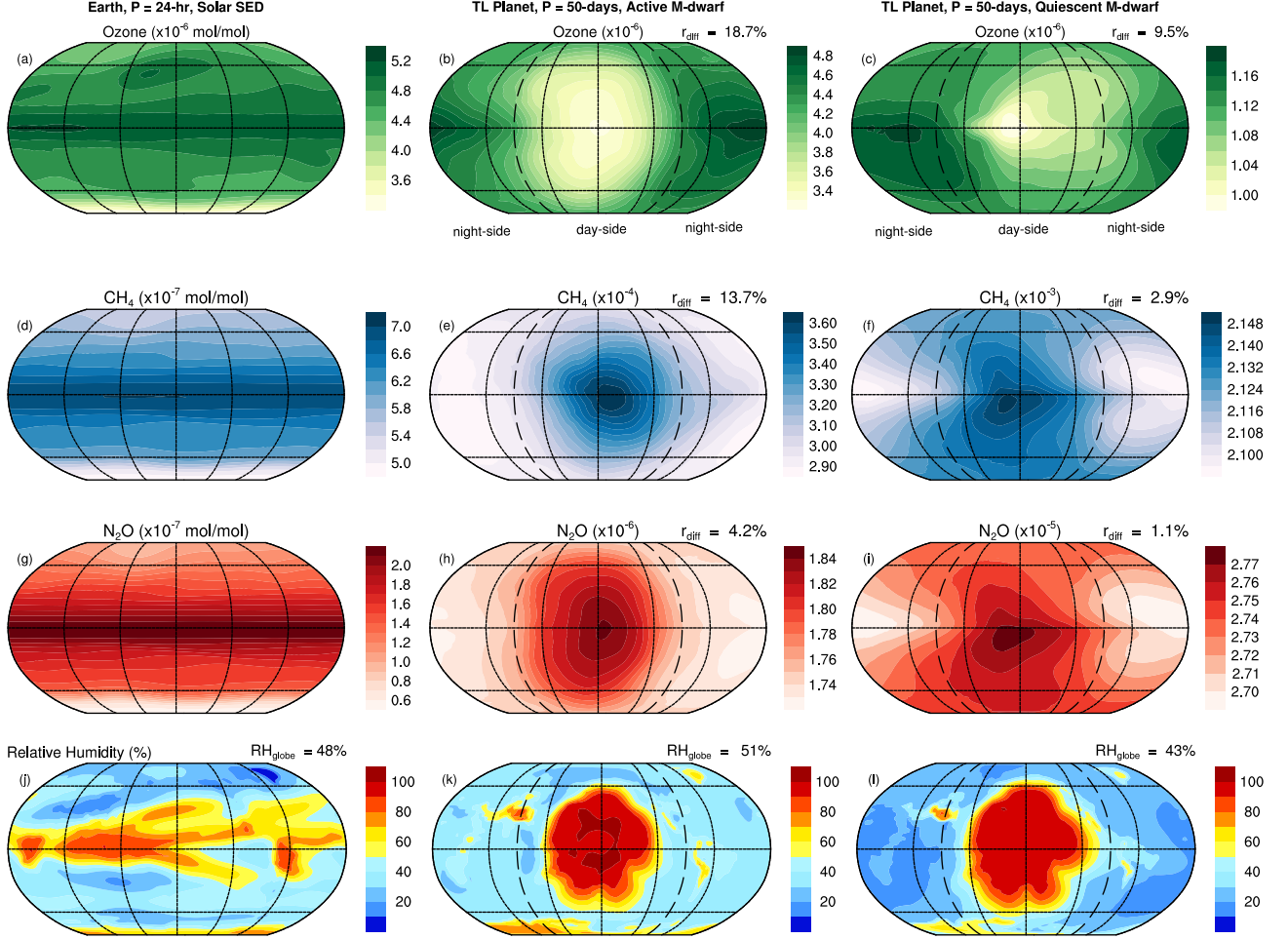


**Figure 1.** Global distribution of O<sub>3</sub>, CH<sub>4</sub>, and N<sub>2</sub>O mixing ratios and relative humidity for Earth-like non-tidally-locked ( $P = 24$  hr) Solar SED simulations (a, d, g, j) and tidally-locked ( $P = 50$  days) active (b, e, h, k) and quiescent (c, f, i, l) M-dwarf SED simulations. Evidence of circulation- and photochemical-induced biosignature anisotropy are apparent. Day-to-night side mixing ratio contrasts ( $r_{\text{diff}}$ ) for tidally-locked simulations are reported, while relative humidity is averaged across the globe ( $\text{RH}_{\text{globe}}$ ). Gas mixing ratios are pressure-weighted vertical averages over the top of the model atmosphere (1-to-100 mb). Relative humidity is reported for the 200 mb pressure surface. Note differences in scaling factors used amongst experiments and constituents. Dashed-lines indicate locations of terminators.

ratio mean,  $r_{\text{night}}$  the nightside mean, and  $r_{\text{globe}}$  the global mean. The degree of anisotropy is loosely encapsulated in this parameter, which is analogous to the definition used by Koll and Abbot (2016) in the context of temperature contrasts. Values of  $r_{\text{diff}}$  for each respective experiment are shown in Figures 1 and 4 and will be discussed throughout the paper.

### 3.1. Ozone Distributions, Water Vapor Mixing Ratios, and Temperature Profiles

Ozone production and destruction depend on stellar UV activity, availability of molecular and atomic oxygen, and ambient meteorological conditions ( $P, T$ ). As our simulated M-dwarf SED is moderately active in the UV bands, our results show similar quantities of ozone

between the baseline Earth-Sun and tidally-locked cases (Figures 1a-c). However, the quiescent SED, produces lower ozone concentrations above the tropopause (Figure 3c). These differences reflect specific stellar activity inputs. Quiescent M-dwarfs emit lower UV in the range responsible for ozone production ( $160 < \lambda < 240$  nm). Moreover, calculated day-to-night side mixing ratio differences  $r_{\text{diff}}$  are higher ( $\sim 19\%$ ) in the active M-dwarf SED scenario, a result of the more photochemically active substellar hemisphere.

Modulations to ozone concentration have major influences on distributions of other biosignature gases. This is due to substellar hemispheric production of excited state atomic oxygen O(<sup>1</sup>D) and constituent families of HO<sub>x</sub>. Both O(<sup>1</sup>D) and HO<sub>x</sub> constituents are reac-

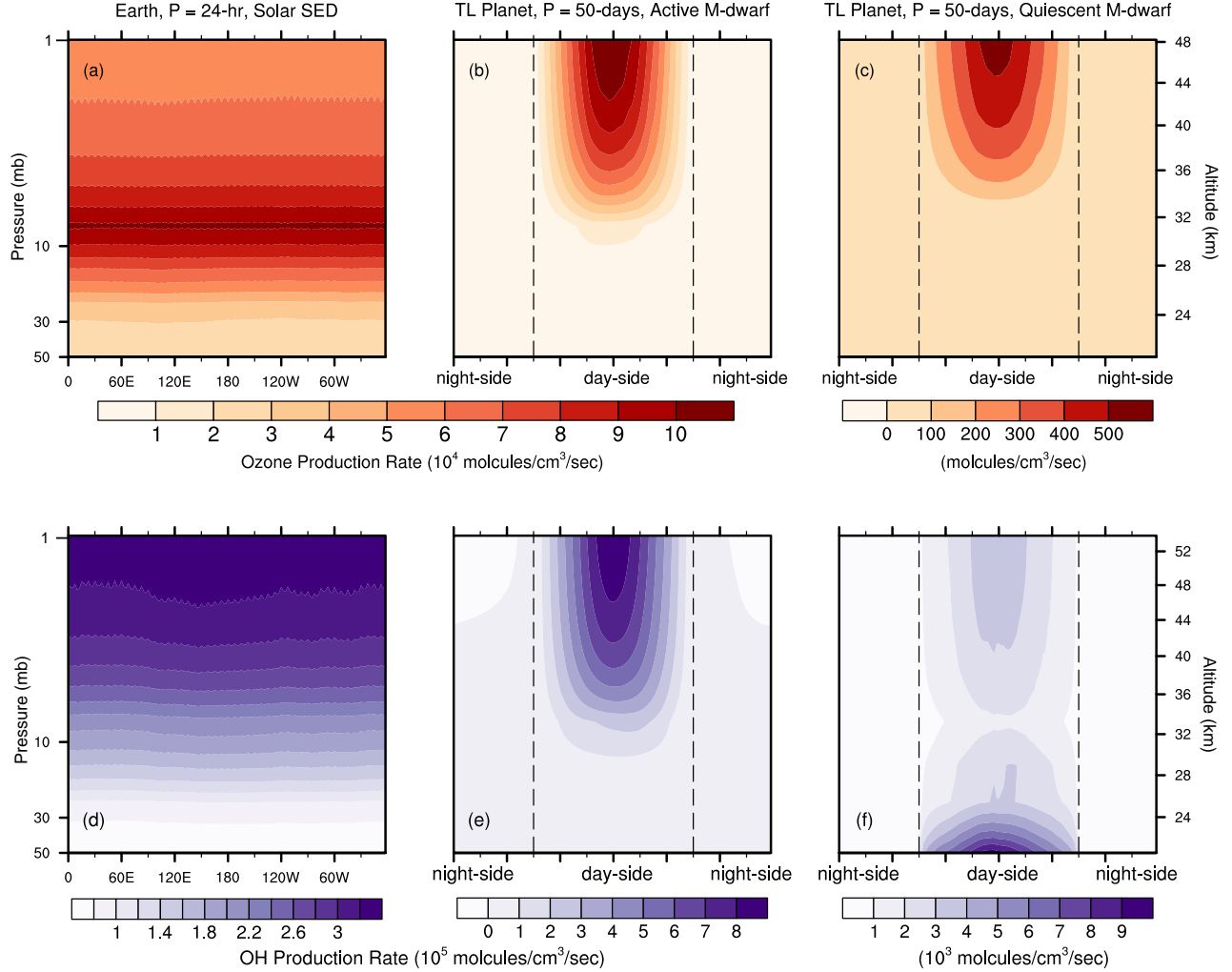
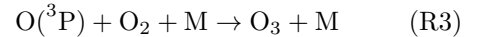
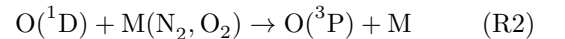
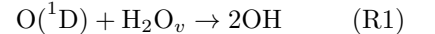


**Figure 2.** Stratospheric  $O_3$  and OH production rates as functions of longitude for Earth-like non-tidally-locked ( $P = 24$  hr) Solar SED simulations (a, d) and tidally-locked ( $P = 50$  days) M-dwarf SED (b, c, e, f) simulations. Photolytic processes drive ozone and hydroxyl radical production and help to explain many of the observed biosignature gas distributions in Figure 1. Note vertical axis begins at 50 mb ( $\sim 20$  km). Dashed-lines indicate locations of terminators.

tive radicals important for atmospheric biogenic organo-compounds and hydrocarbons (e.g.,  $CH_4$ ,  $CH_3$ ,  $HCL$ ,  $H_2S$ ).

As ozone is photochemically produced, horizontal advection carries a portion to the nightside as evidenced by its presence in both hemispheres. The lifetime of ozone ( $\sim 15$  days), in conjunction with day-to-nightside transport, is sufficient enough to sustain some nightside  $O_3$ , but not efficient enough to fully mix the atmosphere, allowing day-to-nightside contrast ( $\sim 19\%$ ; Figure 1b). Conversely, the product  $O(^1D)$  shows limited transport effects due to a short lifetime ( $< 5$  secs), reflected in its large  $r_{diff}$  value ( $\sim 300\%$ ; not shown).  $O(^1D)$  is rapidly removed by one of R1 or R2 reaction pathways (Jacob 1999):



The higher ozone mixing ratios on tidally-locked nightsides is explained by these reaction pathways (Figure 1b-c). Reaction R1, which creates the hydroxyl radical OH, predominantly occurs on the dayside due to the abundance of  $H_2O_v$  (Figures 2e-f). In R2, singlet oxygen returns to the triplet ground state, which can then recombine with oxygen to form ozone via R3. Considered together, significant dayside UV ozone destruction and enhanced removal of  $O(^1D)$  by water

vapor offset higher ozone production rates (Figure 3b), which helps to explain lower dayside ozone mixing ratios (Figure 1b-c).

Interaction of stellar UV photons with  $O_2$  and  $O_3$  can also be seen in vertical temperature profiles. On Earth-like planets, stratospheric temperature is primarily a function of incident UV flux ( $200 < \lambda < 310$  nm) due to the role of  $O_3$  absorption of shortwave photons. In our simulations, this feature is apparent in global and hemispherically averaged profiles. Our simulations indicate that upper-stratospheric temperatures increase (and inversions weaken) as UV radiation levels increase; from quiescent SED, to active SED, to the baseline Earth simulation (Figure 3a). Enhanced UV absorption by  $O_3$  and  $O_2$  increase temperatures above the tropopause, reducing the vertical gradient and inversion strength.

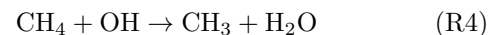
We now turn to discussing testability of our 3D model predictions. Based on simulated ozone distributions, the calculated  $r_{\text{diff}}$  ( $\sim 20\%$ ) is notable but unlikely to be discernible with current observational capabilities (Burrrows 2014). However, this task may prove viable using future instruments (e.g., Greene et al. 2016). Proedrou and Hocke (2016) reached a similar conclusion by comparing total column ozone of a tidally-locked Solar SED Earth and found an  $\sim 23\%$  difference between mean ozone columns during four arbitrary phases due to varying viewing angles.

Compared with 1D model studies, our 3D simulations produce similar ozone mixing ratios (Table 1). However, we find substantially different Bond albedos, temperature, and water mixing ratio profiles. As a consequence of increased dayside water vapor-induced opacity and substellar clouds on tidally-locked planets, global-mean surface temperatures of both tidally-locked simulations are  $\sim 40$  K colder than the baseline (Figure 3a), while Bond albedos are substantially higher (Table 1), in agreement with GCM studies (Yang et al. 2013; Kopparapu et al. 2016, 2017). Colder global (and nightside) temperatures produce lower global water vapor mixing ratios than predicted by 1D models with clear-sky assumptions (i.e., pure water vapor without clouds). Conversely, dayside  $H_2O_v$  mixing ratios are greater due to humid updrafts at the substellar point (Figures 1j-l). Curiously, the quiescent M-dwarf SED simulation (Figure 1l) has lower global-mean relative humidity than the Earth-analog (Figure 1j) and the active M-dwarf case (Figure 1k). This is due to increased ozone mixing ratios and degree of UV absorption, which limit the photolysis of  $H_2O_v$ , in the more active SED simulations. Hence counterintuitively, more dayside  $H_2O_v$  destruction is experienced by the simulation under lower UV radiation. Such behaviors exemplify the value of CCM simulations,

in which capturing feedbacks between 3D dynamical processes, solar forcing, and atmospheric chemistry is critical.

### 3.2. Types I and II Biosignatures: 3D $CH_4$ and $N_2O$ Abundances

$CH_4$  and  $N_2O$  are important biosignatures produced by a myriad of bacterial metabolic pathways (Des Marais et al. 2002; Schwieterman et al. 2018). In Figures 1d-f, we show modeled  $CH_4$  distributions. High  $CH_4$  mixing ratios for planets orbiting quiet M-dwarfs were first noted by Segura et al. (2005) using a 1D model, caused by reduced photochemical removal by reaction with OH:



In our 3D CCM, we find similar global mean  $CH_4$  increases in tidally-locked simulations (Figures 1e-f). However, active and quiescent simulations have low  $CH_4$   $r_{\text{diff}}$  values (13.7% and 2.9%, respectively). Low  $r_{\text{diff}}$  values are explained by a mixture of competing processes. First, upwelling in tidally-locked simulations occurs exclusively below the substellar point, as evidenced by upper-tropospheric moisture patterns (Figures 1j-l). Compared to the baseline, tidally-locked meridional overturning circulation is strengthened, which brings greater moisture aloft. This, in conjunction with the dayside abundance of OH, removes  $CH_4$  via R4. Increased dayside OH production (Figures 2e-f) is a consequence of abundant  $O(^1D)$  and  $H_2O_v$  (R1), both of which are sparse on the nightside. These processes combine to limit dayside  $CH_4$  and produce lower  $r_{\text{diff}}$  values than expected.

$N_2O$  is primarily destroyed by UV photons ( $\lambda < 220$  nm) and photo-oxidation by reactions with stratospheric  $O(^1D)$  (Figure 1g-i). Hence predicted  $N_2O$  concentrations around active M-dwarfs are lesser than those with quiescent SEDs. For both active and quiescent SED simulations, higher concentrations within the substellar hemisphere are found (Figures 1h-i), similar to  $CH_4$  behavior.

Interestingly, simulations forced by the active SED have greater stratospheric  $r_{\text{diff}}$  ( $CH_4$ : 13.7% and  $N_2O$ : 6.9%; Figures 1e-h) than those forced by quiescent SEDs ( $CH_4$ : 2.9% and  $N_2O$ : 1.1%; Figures 1f-i). Higher  $r_{\text{diff}}$  values for active SED cases is somewhat counterintuitive as one might expect that enhanced photolytic destruction on planets around active M-dwarfs should suppress day-to-nightside contrasts. However, simulations forced by active SEDs have more isothermal atmospheres (i.e., weaker temperature inversions; Figure 3a),

### Global-mean and Hemispheric-Mean Vertical Profiles

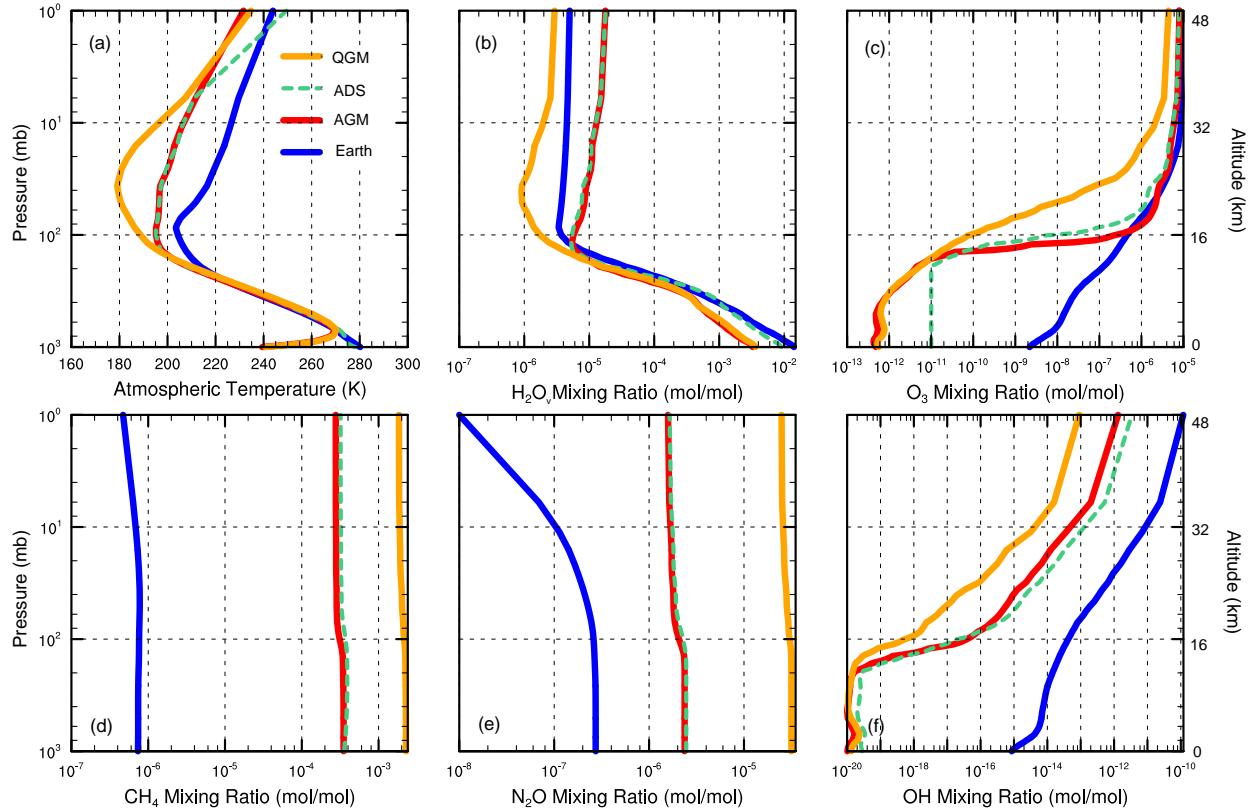


**Figure 3.** Vertical profiles of global-mean temperature (a) and mixing ratios of various gas phase species (b, c, d, e, f). QGM (quiescent global-mean) denotes global-mean values from simulations forced by a quiescent M-dwarf SED, AGM (active global-mean) denotes those forced by an active M-dwarf SED, and ADS (active day-side) denotes dayside-mean values from simulations forced by an active M-dwarf SED. Note axes are log-scaled and begin at planetary surfaces ( $\sim 1000$  mb).

which promote vertical mixing of surface gases above the tropopause, contributing to higher  $r_{\text{diff}}$  values.

#### 3.3. Effects of Surface Fluxes on Atmospheric Distribution: Case of Dimethyl Sulfide

On tidally-locked planets, phototrophs are unlikely to emit biogenic gases globally (i.e., the assumption for all biosignature gases considered thus far); rather, photosynthetically-derived emissions are likely to be restricted to the dayside. To see how a biosignature gas (e.g., DMS;  $\text{C}_2\text{H}_6\text{S}$ ) may behave on a tidally-locked planet, we conduct three experiments, each with a different DMS flux distribution assumption, i.e., Earth-like, tidally-locked with global DMS flux, and tidally-locked with dayside DMS flux (Figure 4). We find that global DMS emissions result in substantially lower  $r_{\text{diff}}$  values ( $\sim 0\%$  and  $\sim 33\%$ ; Figures 4a-b) compared to a strictly dayside DMS emission assumption ( $\sim 67\%$ ; Figure 4c). The larger value of  $r_{\text{diff}}$  in the latter simulation is due

to the relatively short lifetime of DMS (Kloster et al. 2005).

Similar to the above DMS behavior, a potential consequence of tidal-locking is the relegation of  $\text{CH}_4$  and  $\text{N}_2\text{O}$  production to a single hemisphere, i.e., processes of methanogenesis and denitrification favor anaerobic conditions and may be disfavored on photosynthetic oxygen-producing daysides. Spatially-variable surface to atmosphere flux distributions of  $\text{CH}_4$  and  $\text{N}_2\text{O}$  therefore could exhibit higher  $r_{\text{diff}}$  than the values predicted here ( $\lesssim 10\%$ ; Figures 1e-f and 1h-i).

#### 4. DISCUSSION

Here we discuss possible areas of future advancement, as well as the observational relevance of this study.

In this CCM study, we find that factors that determine biosignature concentration and distribution on a habitable tidally-locked planet are species dependent. For example, ozone mixing ratios are primarily driven by photolytic production and destruction, while ozone



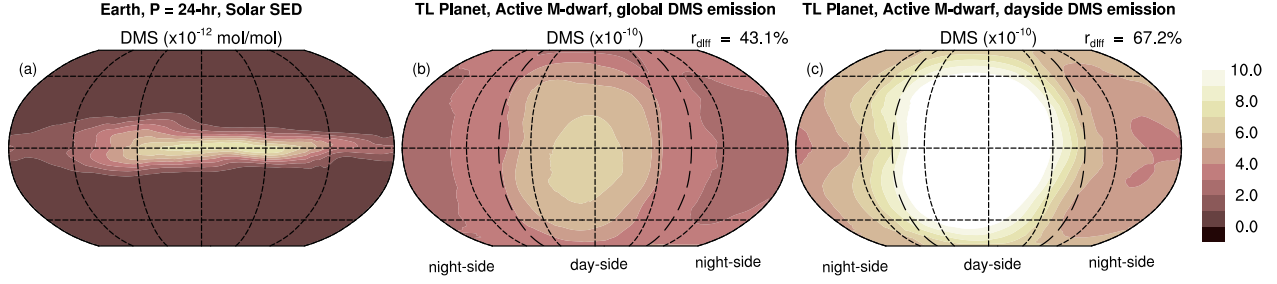


**Figure 4.** Global distribution of photosynthetic biosignature dimethyl sulfide (DMS,  $(\text{CH}_3)_2\text{S}$ ) for Earth-like non-tidally-locked ( $P = 24$  hr) Solar SED simulations (a), tidally-locked ( $P = 50$  days) active M-dwarf SED simulations with a global DMS flux assumption (b), and tidally-locked with a dayside DMS flux assumption (c). Day-to-nightside mixing ratio differences ( $r_{\text{diff}}$ ) for the tidally-locked simulations are reported. Phototrophs are assumed to be only present on the permanently lit day-side in panel (c), which results in an enhanced stratospheric day-to-nightside mixing ratio contrast. Dashed-lines indicate locations of terminators.

distribution and nightside sustenance are controlled by its transport and lifetime. An additional consideration, here demonstrated in our DMS simulations, is the spatial variance of gas fluxes. Given that habitable exoplanets are likely to possess heterogeneous ecologies, whose fluxes will interface with attendant atmospheric structure and circulation patterns, spatially-heterogeneous surface fluxes could have observationally-distinguishable effects on atmospheric spectra. For example, dayside upwelling could facilitate vertical mixing of surface gases into the upper atmosphere (Figure 1e-f), while nightside radiation inversions could trap constituents near the surface, limiting vertical mixing, day-nightside interactions, and potentially observability. These scenarios, in which atmospheric dynamics, photochemistry, surface flux sources, and feedback processes play important roles highlight the utility of 3D CCM simulations. However, due to non-linear interactions and internal atmospheric variability, disentangling drivers of emergent behavior is challenging and will likely require the tools of modern atmospheric and computational science, including Lagrangian tracking of constituents (e.g., Sölch and Kärcher 2010), single- and multi-model ensembles (e.g., Kay et al. 2015), and statistical analyses focused on detection and attribution (e.g., Horton et al. 2015; Diffenbaugh et al. 2017).

Despite these challenges, the introduction of 3D CCMs to exoplanet biosignature prediction efforts offers substantial research potential. Future applications are likely to consider a wider variety of Earth-like biospheres, e.g., markedly disparate atmospheres of Earth throughout geologic time (Rugheimer and Kaltenecker 2018; Arney et al. 2016), and should be expanded to include biologically constrained models and modules (Catling et al. 2018; Walker et al. 2018). Such applications will facilitate egocentricity avoidance – a commonly acknowledged goal of the field (e.g., Seager

et al. 2013). Until then, use of default Earth conditions may restrict the relevance of 3D CCM findings to truly Earth-like planets, with similar atmospheric formation histories, ecospheres, and biological signatures resulting from oxygenic photosynthesis (Meadows et al. 2018).

This study demonstrates that fully-coupled CCMs are particularly promising for studies that seek to assess the roles of and feedbacks between different stellar SEDs, biological behaviors, and atmospheric compositions. Such efforts are consistent with recent reviews, discussing aspirational goals and the future of exoplanet biosignature research (Catling et al. 2018; Walker et al. 2018). Extrasolar astrophysical radiation environments and/or atmospheric conditions may alter biological activity, as life is both photochemically and climatologically mediated. Living organisms are highly receptive toward UV emissions such that UV-B ( $290 < \lambda < 320$  nm) photons hinder metabolism, photosynthesis, and thus biological production rates (?). Moreover, due to different climate and redox conditions, for example on anoxic Archean Earth ( $\sim 3.0$  Ga), hydrocarbons and organosulfur biosignatures ( $\text{C}_2\text{H}_6$ ,  $\text{CH}_4$ ,  $\text{OCS}$ , DMS etc.) could rise to more prominent abundances and hence may be conducive to remote detection (Haqq-Misra et al. 2008; Domagal-Goldman et al. 2011; Hu et al. 2012; Arney et al. 2016).

In terms of the potential observational implications of our simulations, our results agree with those of Segura et al. (2005), Rauer et al. (2011), and Rugheimer et al. (2015), i.e., rocky planets orbiting active and quiet M-dwarfs should have deeper absorption depths, particularly for ozone and secondary biosignatures such as methane and nitrous oxide (as seen in transit and emission spectra). This makes habitable zone planets orbiting M-dwarfs favorable targets. 3D predictions from our CCM simulations may be confirmed by remote observations. Phase curve analysis can potentially resolve 3D

atmospheric structures of super-Earth and Earth-sized terrestrial planets (Stevenson et al. 2014; Kreidberg and Loeb 2016). For example, thick substellar clouds could appear characteristically for planets with specific spin-orbit resonances (Yang et al. 2013).

In terms of biosignature measurements on tidally-locked planets, different longitudinal gradients of gaseous constituents may affect measurements of variation spectra (peak amplitude of the phase curves) extracted from thermal phase curves (Selsis et al. 2011). As variation spectral signals depend on amplitude-peaks in orbital light curves, there may be added anisotropy due to time-varying longitudinal gas distributions on tidally-locked planets in each orbit (assuming null obliquity, as seen in Figure 1). Compared to non-tidally locked fast rotators (with similar stellar UV activity and orbital period), we predict that more pronounced absorption signals would be seen in variation spectrum on tidally-locked planets, driven by greater difference between maximum and minimum phase amplitudes due to uneven hemispheric gas distributions. Emission spectrum at maximum phase (direct line-of-sight) should correspondingly see similar behavior, at least for a few IR-windows (e.g., between 3-9  $\mu\text{m}$ ; Selsis et al. 2011). For direct imaging, one possibility is that these features may be more prominent during certain orbital phases. Ozone observability, for example, may decrease during secondary eclipses as the dayside with reduced ozone abundance would be Earth-facing. Radiative transfer models, using our CCM results as inputs, will be needed to quantitatively assess observational prospects of the above.

## 5. CONCLUSIONS

This Letter reports numerical simulations using a coupled 3D CCM to explore global distribution of biosignature gases on Earth-like and tidally-locked planets as a function of stellar spectral type, stellar activity, and planetary rotation period. Qualitatively similar to 1D models, we find increased mixing ratios of biogenic compounds (e.g.,  $\text{O}_3$ ,  $\text{CH}_4$ , and  $\text{N}_2\text{O}$ ) for both active and inactive M-dwarf SEDs. These increases are most pronounced for planets around quiet M-dwarfs. Even though the effects of tidal-locking are noticeable in our simulations, they are not yet discernable with current observational techniques, i.e., the primary biosignatures simulated in this work ( $\text{O}_3$ ,  $\text{CH}_4$ ,  $\text{N}_2\text{O}$ ) show low ( $\lesssim 20\%$ ) day-to-nightside mixing ratio contrasts. Conversely, simulated day-to-nightside differences of photosynthetic compounds (e.g., DMS) are found to be nearly 70% and underscore the need for heterogeneous 3D realism in modeling biosignatures and their photochemical derivatives. Overall, this study serves as a stepping stone for future applications using 3D CCMs to study the habitability and spectroscopic observability of terrestrial exoplanets.

H.C. thanks J. Schnell and A. Loeb for helpful discussions. E.T.W. thanks NASA Habitable Worlds Grant 80NSSC17K0257 for support. Goddard affiliates are thankful for support from GSFC Sellers Exoplanet Environments Collaboration (SEEC), which is funded by the NASA Planetary Science Divisions Internal Scientist Funding Mode. The VPL team at the University of Washington is thanked for the stellar spectra data. Computational, storage, and staff resources were provided by the QUEST high performance computing facility at Northwestern University, which is jointly supported by the Office of the Provost, Office for Research, and Northwestern University Information Technology.

## REFERENCES

- Anglada-Escudé, Guillem, Pedro J Amado, John Barnes, Zaira M Berdiñas, R Paul Butler, Gavin AL Coleman, Ignacio de La Cueva, Stefan Dreizler, Michael Endl, Benjamin Giesers, et al. “A terrestrial planet candidate in a temperate orbit around Proxima Centauri.” *Nature* 536 (2016): 437–440.
- Arney, G., S. D. Domagal-Goldman, V. S. Meadows, E. T. Wolf, E. Schwieterman, B. Charnay, M. Claire, E. Hébrard, and M. G. Trainer. “The Pale Orange Dot: The Spectrum and Habitability of Hazy Archean Earth.” *Astrobiology* 16 (November 2016): 873–899.
- Barclay, T., J. Pepper, and E. V. Quintana. “A Revised Exoplanet Yield from the Transiting Exoplanet Survey Satellite (TESS).” *ArXiv e-prints* (April 2018).
- Batalha, N. E., N. K. Lewis, M. R. Line, J. Valenti, and K. Stevenson. “Strategies for Constraining the Atmospheres of Temperate Terrestrial Planets with JWST.” *ApJL* 856 (April 2018): L34.

- Bolcar, M. R., L. Feinberg, K. France, B. J. Rauscher, D. Redding, and D. Schiminovich. “Initial technology assessment for the Large-Aperture UV-Optical-Infrared (LUVOIR) mission concept study.” *Space Telescopes and Instrumentation 2016: Optical, Infrared, and Millimeter Wave*. July 2016, 99040J.
- Burrows, A. S. “Spectra as windows into exoplanet atmospheres.” *Proceedings of the National Academy of Science* 111 (September 2014): 12601–12609.
- Catling, D. C., J. Krissansen-Totton, N. Y. Kiang, D. Crisp, T. D. Robinson, S. DasSarma, A. J. Rushby, A. Del Genio, W. Bains, and S. Domagal-Goldman. “Exoplanet Biosignatures: A Framework for Their Assessment.” *Astrobiology* 18 (June 2018): 709–738.
- Danabasoglu, Gokhan and Peter R Gent. “Equilibrium climate sensitivity: Is it accurate to use a slab ocean model?.” *Journal of Climate* 22 (2009): 2494–2499.
- Des Marais, D. J., M. O. Harwit, K. W. Jucks, J. F. Kasting, D. N. C. Lin, J. I. Lunine, J. Schneider, S. Seager, W. A. Traub, and N. J. Woolf. “Remote Sensing of Planetary Properties and Biosignatures on Extrasolar Terrestrial Planets.” *Astrobiology* 2 (June 2002): 153–181.
- Diffenbaugh, Noah S, Deepti Singh, Justin S Mankin, Daniel E Horton, Daniel L Swain, Danielle Touma, Allison Charland, Yunjie Liu, Matz Haugen, Michael Tsiang, et al. “Quantifying the influence of global warming on unprecedented extreme climate events.” *Proceedings of the National Academy of Sciences* 114 (2017): 4881–4886.
- Domagal-Goldman, S. D., V. S. Meadows, M. W. Claire, and J. F. Kasting. “Using Biogenic Sulfur Gases as Remotely Detectable Biosignatures on Anoxic Planets.” *Astrobiology* 11 (June 2011): 419–441.
- Dressing, C. D. and D. Charbonneau. “The Occurrence of Potentially Habitable Planets Orbiting M Dwarfs Estimated from the Full Kepler Dataset and an Empirical Measurement of the Detection Sensitivity.” *ApJ* 807 (July 2015): 45.
- Fujii, Y., A. D. Del Genio, and D. S. Amundsen. “NIR-driven Moist Upper Atmospheres of Synchronously Rotating Temperate Terrestrial Exoplanets.” *ApJ* 848 (October 2017): 100.
- Gillon, M., A. H. M. J. Triaud, B.-O. Demory, E. Jehin, E. Agol, K. M. Deck, S. M. Lederer, J. de Wit, A. Burdanov, J. G. Ingalls, E. Bolmont, J. Leconte, S. N. Raymond, F. Selsis, M. Turbet, K. Barkaoui, A. Burgasser, M. R. Burleigh, S. J. Carey, A. Chaushev, C. M. Copperwheat, L. Delrez, C. S. Fernandes, D. L. Holdsworth, E. J. Kotze, V. Van Grootel, Y. Almleaky, Z. Benkhaldoun, P. Magain, and D. Queloz. “Seven temperate terrestrial planets around the nearby ultracool dwarf star TRAPPIST-1.” *Nature* 542 (February 2017): 456–460.
- Greene, T. P., M. R. Line, C. Montero, J. J. Fortney, J. Lustig-Yaeger, and K. Luther. “Characterizing Transiting Exoplanet Atmospheres with JWST.” *ApJ* 817 (January 2016): 17.
- Haqq-Misra, J., E. T. Wolf, M. Joshi, X. Zhang, and R. K. Kopparapu. “Demarcating Circulation Regimes of Synchronously Rotating Terrestrial Planets within the Habitable Zone.” *ApJ* 852 (January 2018): 67.
- Haqq-Misra, J. D., S. D. Domagal-Goldman, P. J. Kasting, and J. F. Kasting. “A Revised, Hazy Methane Greenhouse for the Archean Earth.” *Astrobiology* 8 (December 2008): 1127–1137.
- Henry, T. J., W.-C. Jao, J. P. Subasavage, T. D. Beaulieu, P. A. Ianna, E. Costa, and R. A. Méndez. “The Solar Neighborhood. XVII. Parallax Results from the CTIOPI 0.9 m Program: 20 New Members of the RECONS 10 Parsec Sample.” *AJ* 132 (December 2006): 2360–2371.
- Horton, Daniel E, Nathaniel C Johnson, Deepti Singh, Daniel L Swain, Bala Rajaratnam, and Noah S Diffenbaugh. “Contribution of changes in atmospheric circulation patterns to extreme temperature trends.” *Nature* 522 (2015): 465.
- Hu, R., S. Seager, and W. Bains. “Photochemistry in Terrestrial Exoplanet Atmospheres. I. Photochemistry Model and Benchmark Cases.” *ApJ* 761 (December 2012): 166.
- Jacob, Daniel. *Introduction to atmospheric chemistry*. Princeton University Press, 1999.
- Kasting, J. F., H. Chen, and R. K. Kopparapu. “Stratospheric Temperatures and Water Loss from Moist Greenhouse Atmospheres of Earth-like Planets.” *ApJL* 813 (November 2015): L3.
- Kasting, J. F., J. B. Pollack, and D. Crisp. “Effects of high CO<sub>2</sub> levels on surface temperature and atmospheric oxidation state of the early earth.” *Journal of Atmospheric Chemistry* 1 (1984): 403–428.

- Kay, J.E., C. Deser, A. Phillips, A. Mai, C. Hannay, G. Strand, J.M. Arblaster, S.C. Bates, G. Danabasoglu, J. Edwards, et al. "The Community Earth System Model (CESM) large ensemble project: A community resource for studying climate change in the presence of internal climate variability." *Bulletin of the American Meteorological Society* 96 (2015): 1333–1349.
- Kettle, A.J. and M.O. Andreae. "Flux of dimethylsulfide from the oceans: A comparison of updated data sets and flux models." *Journal of Geophysical Research: Atmospheres* 105 (2000): 26793–26808.
- Kloster, Sylvia, Johann Feichter, Ernst Maier-Reimer, Katharina D. Six, Philip Stier, and Patrick Wetzel. "DMS cycle in the marine ocean-atmosphere system? a global model study." *Biogeosciences Discussions* 2 (2005): 1067–1126.
- Koll, D. D. B. and D. S. Abbot. "Temperature Structure and Atmospheric Circulation of Dry Tidally Locked Rocky Exoplanets." *ApJ* 825 (July 2016): 99.
- Kopparapu, R. k., E. T. Wolf, G. Arney, N. E. Batalha, J. Haqq-Misra, S. L. Grimm, and K. Heng. "Habitable Moist Atmospheres on Terrestrial Planets near the Inner Edge of the Habitable Zone around M Dwarfs." *ApJ* 845 (August 2017): 5.
- Kopparapu, R. k., E. T. Wolf, J. Haqq-Misra, J. Yang, J. F. Kasting, V. Meadows, R. Terrien, and S. Mahadevan. "The Inner Edge of the Habitable Zone for Synchronously Rotating Planets around Low-mass Stars Using General Circulation Models." *ApJ* 819 (March 2016): 84.
- Kreidberg, L. and A. Loeb. "Prospects for Characterizing the Atmosphere of Proxima Centauri b." *ApJL* 832 (November 2016): L12.
- Lamarque, J.-F., L. K. Emmons, P. G. Hess, D. E. Kinnison, S. Tilmes, F. Vitt, C. L. Heald, E. A. Holland, P. H. Lauritzen, J. Neu, J. J. Orlando, P. J. Rasch, and G. K. Tyndall. "CAM-chem: description and evaluation of interactive atmospheric chemistry in the Community Earth System Model." *Geoscientific Model Development* 5 (March 2012): 369–411.
- Lean, Judith, Juerg Beer, and Raymond Bradley. "Reconstruction of solar irradiance since 1610: Implications for climate change." *Geophysical Research Letters* 22 (1995): 3195–3198.
- Lewis, N. T., F. H. Lambert, I. A. Boutle, N. J. Mayne, J. Manners, and D. M. Acreman. "The Influence of a Substellar Continent on the Climate of a Tidally Locked Exoplanet." *ApJ* 854 (February 2018): 171.
- Lovelock, J. E. "Thermodynamics and the Recognition of Alien Biospheres." *Proceedings of the Royal Society of London Series B* 189 (May 1975): 167–180.
- MacFarling Meure, C., D. Etheridge, C. Trudinger, P. Steele, R. Langenfelds, T. Van Ommen, A. Smith, and J. Elkins. "Law Dome CO<sub>2</sub>, CH<sub>4</sub> and N<sub>2</sub>O ice core records extended to 2000 years BP." *Geophysical Research Letters* 33 (2006).
- Mann, A. W., G. A. Feiden, E. Gaidos, T. Boyajian, and K. von Braun. "How to Constrain Your M Dwarf: Measuring Effective Temperature, Bolometric Luminosity, Mass, and Radius." *ApJ* 804 (May 2015): 64.
- Meadows, V. S., G. N. Arney, E. W. Schwieterman, J. Lustig-Yaeger, A. P. Lincowski, T. Robinson, S. D. Domagal-Goldman, R. Deitrick, R. K. Barnes, D. P. Fleming, R. Luger, P. E. Driscoll, T. R. Quinn, and D. Crisp. "The Habitability of Proxima Centauri b: Environmental States and Observational Discriminants." *Astrobiology* 18 (February 2018): 133–189.
- Meadows, V. S., C. T. Reinhard, G. N. Arney, M. N. Parenteau, E. W. Schwieterman, S. D. Domagal-Goldman, A. P. Lincowski, K. R. Stapelfeldt, H. Rauer, S. DasSarma, S. Hegde, N. Narita, R. Deitrick, J. Lustig-Yaeger, T. W. Lyons, N. Siegler, and J. L. Grenfell. "Exoplanet Biosignatures: Understanding Oxygen as a Biosignature in the Context of Its Environment." *Astrobiology* 18 (June 2018): 630–662.
- Mennesson, B., S. Gaudi, S. Seager, K. Cahoy, S. Domagal-Goldman, L. Feinberg, O. Guyon, J. Kasdin, C. Marois, D. Mawet, M. Tamura, D. Mouillet, T. Prusti, A. Quirrenbach, T. Robinson, L. Rogers, P. Scowen, R. Somerville, K. Stapelfeldt, D. Stern, M. Still, M. Turnbull, J. Booth, A. Kiessling, G. Kuan, and K. Warfield. "The Habitable Exoplanet (HabEx) Imaging Mission: preliminary science drivers and technical requirements." *Space Telescopes and Instrumentation 2016: Optical, Infrared, and Millimeter Wave*. July 2016, 99040L.
- Neale, Richard B., Chih-Chieh Chen, Andrew Gettelman, Peter H. Lauritzen, Sungsu Park, David L. Williamson, Andrew J. Conley, Rolando Garcia, Doug Kinnison, Jean-Francois Lamarque, et al. "Description of the NCAR community atmosphere model (CAM 5.0)." *NCAR Tech. Note NCAR/TN-486+STR* 1 (2010): 1–12.
- Proedrou, E. and K. Hocke. "Characterising the three-dimensional ozone distribution of a tidally locked Earth-like planet." *Earth, Planets, and Space* 68 (June 2016): 96.

- Rauer, H., S. Gebauer, P. V. Paris, J. Cabrera, M. Godolt, J. L. Grenfell, A. Belu, F. Selsis, P. Hedelt, and F. Schreier. “Potential biosignatures in super-Earth atmospheres. I. Spectral appearance of super-Earths around M dwarfs.” *A&A* 529 (May 2011): A8.
- Rugheimer, S. and L. Kaltenegger. “Spectra of Earth-like Planets through Geological Evolution around FGKM Stars.” *ApJ* 854 (February 2018): 19.
- Rugheimer, S., L. Kaltenegger, A. Segura, J. Linsky, and S. Mohanty. “Effect of UV Radiation on the Spectral Fingerprints of Earth-like Planets Orbiting M Stars.” *ApJ* 809 (August 2015): 57.
- Sagan, C., W. R. Thompson, R. Carlson, D. Gurnett, and C. Hord. “A search for life on Earth from the Galileo spacecraft.” *Nature* 365 (October 1993): 715–721.
- Schwieterman, E. W., N. Y. Kiang, M. N. Parenteau, C. E. Harman, S. DasSarma, T. M. Fisher, G. N. Arney, H. E. Hartnett, C. T. Reinhard, S. L. Olson, V. S. Meadows, C. S. Cockell, S. I. Walker, J. L. Grenfell, S. Hegde, S. Rugheimer, R. Hu, and T. W. Lyons. “Exoplanet Biosignatures: A Review of Remotely Detectable Signs of Life.” *Astrobiology* 18 (June 2018): 663–708.
- Seager, S., W. Bains, and R. Hu. “A Biomass-based Model to Estimate the Plausibility of Exoplanet Biosignature Gases.” *ApJ* 775 (October 2013): 104.
- Seager, S., D. Deming, and J. A. Valenti. “Transiting Exoplanets with JWST.” *Astrophysics and Space Science Proceedings* 10 (2009): 123.
- Segura, A., J. F. Kasting, V. Meadows, M. Cohen, J. Scalo, D. Crisp, R. A. H. Butler, and G. Tinetti. “Biosignatures from Earth-Like Planets Around M Dwarfs.” *Astrobiology* 5 (December 2005): 706–725.
- Seinfeld, John H and Spyros N Pandis. *Atmospheric chemistry and physics: from air pollution to climate change*. John Wiley & Sons, 2012.
- Selsis, F., R. D. Wordsworth, and F. Forget. “Thermal phase curves of nontransiting terrestrial exoplanets. I. Characterizing atmospheres.” *A&A* 532 (August 2011): A1.
- Shields, A. L., C. M. Bitz, V. S. Meadows, M. M. Joshi, and T. D. Robinson. “Spectrum-driven Planetary Deglaciation due to Increases in Stellar Luminosity.” *ApJL* 785 (April 2014): L9.
- Sölch, Ingo and Bernd Kärcher. “A large-eddy model for cirrus clouds with explicit aerosol and ice microphysics and Lagrangian ice particle tracking.” *Quarterly Journal of the Royal Meteorological Society* 136 (2010): 2074–2093.
- Stevenson, K. B., J.-M. Désert, M. R. Line, J. L. Bean, J. J. Fortney, A. P. Showman, T. Kataria, L. Kreidberg, P. R. McCullough, G. W. Henry, D. Charbonneau, A. Burrows, S. Seager, N. Madhusudhan, M. H. Williamson, and D. Homeier. “Thermal structure of an exoplanet atmosphere from phase-resolved emission spectroscopy.” *Science* 346 (November 2014): 838–841.
- Tarter, J. C., P. R. Backus, R. L. Mancinelli, J. M. Aurnou, D. E. Backman, G. S. Basri, A. P. Boss, A. Clarke, D. Deming, L. R. Doyle, E. D. Feigelson, F. Freund, D. H. Grinspoon, R. M. Haberle, S. A. Hauck, II, M. J. Heath, T. J. Henry, J. L. Hollingsworth, M. M. Joshi, S. Kilston, M. C. Liu, E. Meikle, I. N. Reid, L. J. Rothschild, J. Scalo, A. Segura, C. M. Tang, J. M. Tiedje, M. C. Turnbull, L. M. Walkowicz, A. L. Weber, and R. E. Young. “A Reappraisal of The Habitability of Planets around M Dwarf Stars.” *Astrobiology* 7 (March 2007): 30–65.
- Taylor, Karl E, Ronald J Stouffer, and Gerald A Meehl. “An overview of CMIP5 and the experiment design.” *Bulletin of the American Meteorological Society* 93 (2012): 485–498.
- Thompson, S. E., J. L. Coughlin, K. Hoffman, F. Mullally, J. L. Christiansen, C. J. Burke, S. Bryson, N. Batalha, M. R. Haas, J. Catanzarite, J. F. Rowe, G. Barentsen, D. A. Caldwell, B. D. Clarke, J. M. Jenkins, J. Li, D. W. Latham, J. J. Lissauer, S. Mathur, R. L. Morris, S. E. Seader, J. C. Smith, T. C. Klaus, J. D. Twicken, J. E. Van Cleve, B. Wohler, R. Akeson, D. R. Ciardi, W. D. Cochran, C. E. Henze, S. B. Howell, D. Huber, A. Prša, S. V. Ramírez, T. D. Morton, T. Barclay, J. R. Campbell, W. J. Chaplin, D. Charbonneau, J. Christensen-Dalsgaard, J. L. Dotson, L. Doyle, E. W. Dunham, A. K. Dupree, E. B. Ford, J. C. Geary, F. R. Girouard, H. Isaacson, H. Kjeldsen, E. V. Quintana, D. Ragozzine, M. Shabram, A. Shporer, V. Silva Aguirre, J. H. Steffen, M. Still, P. Tenenbaum, W. F. Welsh, A. Wolfgang, K. A. Zamudio, D. G. Koch, and W. J. Borucki. “Planetary Candidates Observed by Kepler. VIII. A Fully Automated Catalog with Measured Completeness and Reliability Based on Data Release 25.” *ApJS* 235 (April 2018): 38.
- Wakeford, H. R., D. K. Sing, T. Kataria, D. Deming, N. Nikolov, E. D. Lopez, P. Tremblin, D. S. Amundsen, N. K. Lewis, A. M. Mandell, J. J. Fortney, H. Knutson, B. Benneke, and T. M. Evans. “HAT-P-26b: A Neptune-mass exoplanet with a well-constrained heavy element abundance.” *Science* 356 (May 2017): 628–631.



- Walker, S. I., W. Bains, L. Cronin, S. DasSarma, S. Danielache, S. Domagal-Goldman, B. Kacar, N. Y. Kiang, A. Lenardic, C. T. Reinhard, W. Moore, E. W. Schwieterman, E. L. Shkolnik, and H. B. Smith. “Exoplanet Biosignatures: Future Directions.” *Astrobiology* 18 (June 2018): 779–824.
- Way, M. J., A. D. Del Genio, N. Y. Kiang, L. E. Sohl, D. H. Grinspoon, I. Aleinov, M. Kelley, and T. Clune. “Was Venus the first habitable world of our solar system?.” *Geophys. Res. Lett.* 43 (August 2016): 8376–8383.
- Wolf, E. T. “Assessing the Habitability of the TRAPPIST-1 System Using a 3D Climate Model.” *ApJL* 839 (April 2017): L1.
- Wolf, E. T. and O. B. Toon. “The evolution of habitable climates under the brightening Sun.” *Journal of Geophysical Research (Atmospheres)* 120 (June 2015): 5775–5794.
- Wordsworth, R. “Atmospheric Heat Redistribution and Collapse on Tidally Locked Rocky Planets.” *ApJ* 806 (June 2015): 180.
- Yang, J., N. B. Cowan, and D. S. Abbot. “Stabilizing Cloud Feedback Dramatically Expands the Habitable Zone of Tidally Locked Planets.” *ApJL* 771 (July 2013): L45.
- Yang, J., J. Leconte, E. T. Wolf, C. Goldblatt, N. Feldl, T. Merlis, Y. Wang, D. D. B. Koll, F. Ding, F. Forget, and D. S. Abbot. “Differences in Water Vapor Radiative Transfer among 1D Models Can Significantly Affect the Inner Edge of the Habitable Zone.” *ApJ* 826 (August 2016): 222.